Energy and Environment Research; Vol. 10, No. 2; 2020
ISSN 1927-0569 E-ISSN 1927-0577
Published by Canadian Center of Science and Education

Air Flow Model for Mixed-Mode and Indirect-Mode Natural Convection Solar Drying of Maize

Isaac N. Simate[1]

[1] Department of Agricultural Engineering, School of Engineering, University of Zambia, Zambia

Correspondence: Isaac N. Simate, Department of Agricultural Engineering, School of Engineering, University of Zambia, P. O. Box 32379, Lusaka, Zambia. E-mail: isaac.simate@unza.zm

Received: July 8, 2020 Accepted: August 27, 2020 Online Published: September 22, 2020

doi:10.5539/eer.v10n2p1 URL: https://doi.org/10.5539/eer.v10n2p1

Abstract

An air flow model for mixed-mode and indirect-mode natural convection solar drying of maize to help understand the factors that influence air flow in the dryer is presented. Temperatures at various sections of the dryer obtained from drying experiments were input to the air flow model to predict the respective thermal buoyancies. The air flow rate was determined by balancing the sum of the buoyancy pressures with the sum of the flow resistances in the various sections of the dryer. To validate the model, the predicted air flow was compared with measured air flow from experiments. For both the mixed-mode and indirect-mode, the biggest driver of the air flow is the thermal buoyancy created in the collector, while the grain bed is the dominant pressure drop. Thermal buoyancy on top of the grain bed is largely responsible for the variation in air flow, translating into low mass air flow during the early stages of drying when grain moisture is high, and higher air flow in the later stages when grain moisture is low. The heating of the grain bed by direct radiation in the mixed-mode translates into a slightly higher air flow rate than the indirect-mode. The implications are that a thinner grain bed results in shorter drying time as it has a higher air flow rate than a thicker one. To mitigate the low air flow at the early stages of drying, the collector length should be appropriately designed for a desired air flow.

Keywords: air flow model, indirect mode, mixed-mode, natural convection, solar drying

1. Introduction

Mixed-mode and Indirect-mode solar dryers have a separate compartment, the collector, in which the air from ambient is heated before passing through the grain bed. In addition, for the mixed-mode, the top surface of the grain bed is heated directly by solar energy through a transparent cover. The heated air performs two functions: a) it supplies heat for the evaporation of moisture from the grain and, b) it takes away the evaporated moisture (Bala & Woods, 1994). Consequently, for a natural convection solar dryer, the air flow is one of the main factors that affect its performance. A deeper understanding of the behaviour of the air flow at the various sections of the dryer will enable the design of better performance solar dryers. Maundu, Kiptoo, Eliud, Kindole, and Nakajo (2017) studied air flow distribution and velocity across the drying chamber in a natural convection solar dryer by the use of Particle Image Velocimetry technique which is an effective tool in visual analysis of air flow distribution and provides real experimental air flow analysis. Al-Neama and Farkas (2016) modelled air flow in a natural convection solar dryer and showed that the velocity of air in the chimney was a function of temperature change across the chimney. Vintilă, Ghiauş, and Fătu (2014) used computational fluid dynamics to simulate the velocity field, pressure distribution and temperature distribution in the solar collector and in the drying chamber of a solar dryer. Berinyuy, Tangka, and Weka Fotso (2012) used the relationship developed by Brenndorfer et al. (1987), where the air flow is related to the pressure drop across the dryer, and the depth of the material being dried in their design of a natural convection solar tunnel dryer with integrated collector and chimney. Rigit and Low (2010) carried out modelling of velocity distributions inside a natural convection solar dryer using computational fluid dynamics. The maximum air velocity that could be achieved was found at the area near the chimney outlet.

In order to develop an air flow model, the mixed-mode and indirect-mode natural convection solar dryers are studied together to determine and compare the contributions of the sections of each dryer to their air flow. The measurement of air flow can be done with an anemometer, which is a thermal apparatus for the measurement of

fluid flow. According to Benson (1974), the apparatus can be classified into two groups with the first group exploiting the effect of the stream on the temperature of a heated body such as in the hot wire anemometer. In the second group, a certain amount of heat is added to a confined stream and the resultant temperature rise is then used to calculate the mass flow rate. One device in this group, the Thomas flow meter, was devised to measure mass flow rates of gas in pipes. Dunn (2006) reported that anemometers are now widely used and among the many advantages they have is minimal obstruction to flow because of their very small size. Since the air flow rates in natural-convection solar dryers can be very small, in fact, too small to be measured with most flow meters which operate on the principles of obstruction and pressure drop, anemometers with their small probes do not present large obstructions to the flow and are therefore suitable for this work.

The objective of this study is to develop an air flow model for mixed-mode and indirect-mode natural convection solar drying of maize and validate it with experiment.

2. Theory

The laboratory natural convection mixed-mode solar dryer under consideration is illustrated in Figure 1. Under mixed-mode configuration, the dryer has glass covers on both the collector and the drying chamber. To use it as an indirect-mode dryer, the drying chamber glass is covered with plywood to block radiation to the top of the grain bed. The air flow through the solar dryer is initiated by the buoyancy-induced pressure head that is created above the atmospheric pressure. The temperature of air in the collector and drying chamber is higher than that in the ambient. This makes the air inside the collector and drying chamber less dense than that in the ambient and therefore creates the buoyancy pressure.

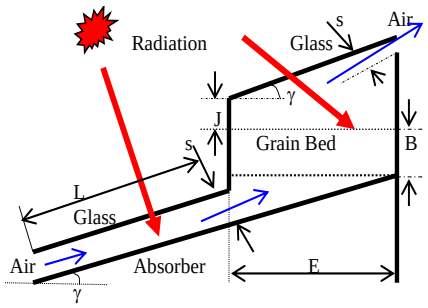

Figure 1. Section through a Mixed-mode Solar Dryer

Note. collector length, L = 1.2 m; collector and drying chamber width, W = 1.0 m; drying chamber length, E = 0.35 m; space above grain bed, J = 0.15 m; collector angle, γ = 18.5°; spacing between absorber and glass cover; and also drying chamber exit vent, s = 0.05 m; grain bed depth, B = 0.04 m for10 kg and 0.02 m for 5 kg capacity) (Simate, 1999).

As the air flows through the dryer, pressure drops occur in the various sections of the dryer such as the collector and the grain bed. The pressure drop across the grain bed is dominant. These pressure drops are equal to the buoyancy induced pressure (Oosthuizen, 1987).

2.1 Air flow Model

By balancing the buoyancy pressure with the flow resistance in the dryer, the air flow rate can be determined from the following equation (Bala & Woods, 1994):

$$TB_{total} = PD_{grain} + PD_{coll} + PD_{exit} \quad (1)$$

where TB_{total}, the total thermal buoyancy pressure, is the sum of the individual thermal buoyancy pressures in the various sections of the dryer, and PD_{grain}, PD_{coll} and PD_{exit} are pressure drops through grain bed, through collector, and at exits of collector and drying chamber, respectively. Each section of the dryer with a vertical height and a mean temperature difference above ambient contributes to the total thermal buoyancy as follows:

2.1.1 Thermal Buoyancy in Collector

The temperature difference between the mean temperature of air in the collector ($T_{collector\ mean}$) and that of ambient (T_{am}) creates the thermal buoyancy pressure in the collector ($TB_{collector}$) and is given by;

$$TB_{collector} = g\beta\rho_a\left(T_{collector\ mean} - T_{am}\right)L\sin\gamma \quad (2)$$

Where L = collector length, m

γ = collector angle to the horizontal, degrees

g = acceleration due to gravity, m/s^2

β = coefficient for thermal expansion, 1/K

ρ_a = density of air, kg/m^3

2.1.2 Thermal Buoyancy in the Space between Collector Exit and Bottom of Grain Bed

Assuming that there are no heat losses in the plenum, the temperature of the air coming out of the collector (T_{out}) is the same as that at the bottom of the grain bed. Therefore, this gives a temperature difference which acts on the vertical height from the bottom of the grain bed to the collector exit and the resulting buoyancy pressure ($TB_{collector\ out}$) is given by;

$$TB_{collector\ out} = g\beta\rho_a(T_{out} - T_{am})E\tan\gamma \tag{3}$$

2.1.3 Thermal Buoyancy on Top of Grain Bed

The air on top of the bed, which comes from within the bed, introduces an additional buoyancy force, a product of the air temperature above that of the ambient (air temperature on top of the grain bed, T_{top}, less the ambient temperature) and the height of the space it occupies. In addition for a mixed-mode solar dryer, the top surface of the grain bed is heated by the solar radiation coming through the transparent drying chamber cover. Consequently, the air entering the dryer, whose temperature may already be higher than that of the ambient, is heated by the grain bed surface. The height of the space above the grain bed varies since the glass cover is at an angle γ with the grain surface and so the height from the grain surface to the drying chamber exit is used to calculate the thermal buoyancy on top of the grain bed ($TB_{top\ grain}$) as follows:

$$TB_{top\ grain} = g\rho_a\beta\left(T_{top} - T_{am}\right)\left(J + E\ \tan(\gamma) - s\right) \tag{4}$$

2.1.4 Thermal Buoyancy in Grain Bed

The final contribution to the buoyancy pressure is created in a grain bed of depth B due to the difference in the density between the hot air contained therein and the ambient. It is given by;

$$TB_{grain} = g\ B(\rho_{am} - \rho_a) \tag{5}$$

where ρ_a = the density of air inside the grain bed

The thermal buoyancy pressure inside the grain bed (TB_{grain}) is finally given as;

$$TB_{grain} = g\ B\ \rho_a\ \beta(T_{av} - T_{am}) \tag{6}$$

where T_{av} = average air temperature in the grain bed.

The pressure drops at different sections of the dryer are given as follows:

2.1.5 Pressure Drop across Grain Bed

The pressure drop across the grain bed is related to the air velocity through the bed and is given by Brooker (1969) as;

$$V_{grain} = A\left(PD_{grain}\right)^R \tag{7}$$

Where V is air velocity through the grain bed in m/min, PD_{grain} is pressure drop across the grain bed in kPa/m, the coefficients are A = 41.0 and R = 0.867, for a range of pressure drop of 0.009 – 0.021 kPa/m.

2.1.6 Pressure Drop across Collector

The pressure drop across the collector (PD_{coll}) is due to the resistance of the inner surface of the collector to air flow and can be expressed from equation (8) (Daly, 1979) as;

$$PD_{coll} = \frac{G^2 f L}{2\rho_a d_h} \tag{8}$$

The friction factor relationships are given by Bayazitoglu and Ozisik (1988) as;

$$f = \frac{64}{\mathrm{Re}} \tag{9}$$

for Re < 4 000, and

$$f = 0.316\,\mathrm{Re}^{-0.25} \tag{10}$$

for 4 000 < Re < 20 000.

2.1.7 Pressure Drop at Collector and Drying Chamber Exits

As the air exits from the collector and from the drying chamber into the atmosphere, a loss in pressure head (PD_{exit}) occurs. This pressure loss is presented here by using the dynamic head loss coefficient K_{ex}, at the exits of the collector and dryer.

$$PD_{exit} = K_{ex} \frac{G^2}{2\rho_a} \tag{11}$$

The dynamic head loss coefficient is obtained from a table of various expansion and contraction geometries as presented by Daly (1979). Values of 0.65 and 1.0 were used for the collector and dryer exits respectively.

2.1.8 Pressure Drop through Perforated Metal Tray

In case of grain on a perforated metal tray, the pressure drop through the perforations is small compared with that through the grain mass if the hole area is 10% or more of the total surface area (Brooker, Bakker-Arkema, & Hall, 1992). The perforated metal base for the tray used in the experiments and in the design had 33% hole area and pressure drop was therefore taken as negligible.

3. Materials and Methods

3.1 Model Prediction and Validation

The data that was used in the model to predict air flow was obtained from drying experiments where maize was dried from a moisture content of 24.7 % to 12.6 % wet basis. For validation, data was obtained from air flow experiments done on dry maize with a moisture content of 13.4 % wet basis. Both experiments were performed using the same dryer and maize variety under similar laboratory conditions of the solar simulator radiation intensity of 634.78 W/m^2 at the University of Newcastle upon Tyne, United Kingdom. Details of both experiments are given in Simate (1999) and Simate (2001).

3.1.1 Model Prediction

Temperatures at various sections of the dryer obtained from the drying experiments were input to the air flow model to predict the thermal buoyancies at various sections of the dryer with respect to elapsed drying time. The total thermal buoyancy (sum of thermal buoyancies at various sections of the dryer) was then balanced with the total pressure drop (sum of pressure drops at various sections of the dryer) in order to determine the mass air flow through the dryer. The above procedure was done in Microsoft Excel.

3.1.2 Model Validation

A thermal apparatus, Thomas flow meter (Benson, 1974), was constructed and coupled to the inlet of the collector of the solar dryer used to measure the air flow. The construction of the Thomas meter involved making a rectangular heater box of 0.5 m length, 1 m width and 0.05 m depth and open at two ends one end of which was aligned and joined to the inlet of the collector. Two sets of type-T thermocouples (measurement range: -200 to 350 ℃; sensitivity: 43 μV/℃; accuracy: ± 0.75 %) were each positioned near each of the two open ends of the heater box. Each set had five thermocouples placed equidistant on an aluminium strip across the 50 mm depth of the heater box. The five thermocouples near the collector inlet formed the hot junctions and were joined, in a differential set up, to their corresponding cold junctions at the other end of the heater box (Figure 2). This set up therefore, constituted five pairs of differential thermocouples. A data logger Campbell Scientific CR10X was used to record the temperatures.

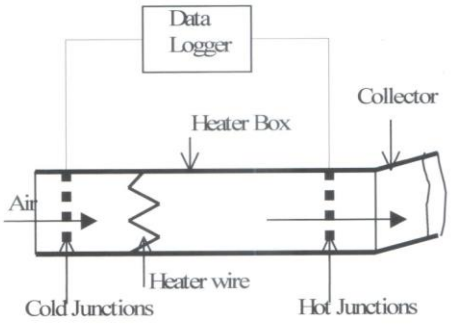

Figure 2. Apparatus for measuring air flow using thermocouples

The heater was made from nichrome wire with a resistance of 47.5 Ω and was placed across the whole width of the heater box between the two sets of thermocouples. The wire was connected to a variable voltage power supply, and a setting of 40 volts was found adequate in order to avoid high radiation losses from the heating wire but at the same time provide enough heat to raise the air temperature by at least 1 ℃. The heater was placed nearer to the inlet of the heater box in order to allow more mixing of the heated and incoming air before the air entered the collector.

The air flow measurements were performed with two grain capacities of 10 kg and 5 kg operating in mixed-mode. After loading grain into the dryer, the solar simulator lights were switched on. The whole solar dryer and in particular the solar collector had to be at the stable operating temperature. Initial calculations showed that the collector had a time constant of about one hour and therefore the whole dryer was allowed to stabilise for this period of time before making any recordings. At the end of the stabilising period, the data logger was switched on to start recording the five differential temperatures every five minutes throughout the experiment. The heater was switched on for 60 minutes but the temperatures were recorded for a total period of 135 minutes with the first 15 minutes and the last 60 minutes when the heater off. This procedure was done for both the 10kg and 5 kg capacity.

The mass air flow rate is given by,

$$\dot{m} = P/(C_{pa}\,\Delta T) \tag{12}$$

where

$\dot{m}$ = the mass air flow rate, kg/s

P = energy input to the heater, W

C_{pa} = specific heat capacity of air, J/kg K

ΔT = temperature difference, ℃

With a 40 volts power supply and a resistance of 47.5 Ω, the energy input to the heater was calculated as 33.67 W. The ΔT was calculated from the graphs of temperature difference with time by taking the difference between the average ΔT with heater on and the average ΔT with heater off for all the 5 differential thermocouples. The specific heat capacity of air was taken as 1005 J/kg/K.

3.2 Uncertainties and Errors in Measured Parameters

The parameter that was measured in these experiments was the air temperature at the cold and hot junctions of the heater box. Errors and uncertainties could have arisen from the design of the experiment, inaccurate reading of instruments, calibration and instrument resolution. Moffat (1988) reported that an estimate of the possible residual error in a measurement, having taken care of all corrections, is the uncertainty attributed to that measurement. Further, the root-sum-square combination of the uncertainties of all the subordinate measurements under consideration in the present measurement is the overall uncertainty of a measurement.

According to NASA (2010), the standard deviation of the sample data is used to determine the uncertainty due to repeatability or random error, while uncertainty due to systematic errors is estimated heuristically from containment limits, containment probability and the inverse error distribution. The uncertainty due to systematic error for a normally distributed error is given by equation (13); for uniformly distributed error it is given by equation (14) and, for overall uncertainty by equation (15);

$$U = \frac{L}{\phi^{-1}\left(\frac{1+p}{2}\right)} \tag{13}$$

Where, $\pm L$ are the containment limits which may be taken from manufacturer tolerance limits, calibration records or certificates, or statistical process control limits; p is the containment probability; and $\phi^{-1}(\,)$ is the inverse normal distribution function.

$$U = \frac{L}{\sqrt{3}} \tag{14}$$

$$U_{overall} = \sqrt{\left\{U_{bias}^2 + U_{random}^2 + U_{resolution}^2 + U_{operator}^2 + U_{environment}^2\right\}} \tag{15}$$

Where: $U_{overall}$ is the overall uncertainty; U_{bias} is the uncertainty due to reference attribute bias and persists during a measurement session; U_{random} is the uncertainty due to repeat measurement and manifests itself as differences in

measured value from measurement to measurement during a measurement session; $U_{resolution}$ is uncertainty due to the smallest discernible value indicated in a measurement; and $U_{operator}$ is uncertainty due to errors introduced by the person taking the measurement and producing a systematic bias towards a measurement; $U_{environment}$ is due to errors introduced by changing environmental conditions such as temperature and humidity.

4. Results and Discussion

4.1 Uncertainty Analyses

The error contributing to measurement bias uncertainty for all the parameters measured was considered to be normally distributed with 97.5 % containment probability. The uncertainty due to reference attribute bias during the measurement session U_{bias} was determined as ± 0.446 ºC from equation (13). For the temperature measurement, this was the only contributor to the overall uncertainty.

The uncertainty due to repeat measurement that manifests itself as differences in measured value from measurement to measurement during a measurement session U_{random} was taken as zero. No repeatability, parameter values changed continuously with time according to the weather conditions.

The uncertainty due to the smallest discernible value indicated in a measurement $U_{resolution}$ was taken as zero since the measurements were recorded automatically in the data logger and computer.

The uncertainty due to errors introduced by the person taking the measurement and producing a systematic bias towards a measurement $U_{operator}$ was taken as zero; the thermocouple were handled/positioned once at start of experiment when positioning them at the measuring point.

The uncertainty due to errors introduced by changing environmental conditions such as temperature and humidity $U_{environment}$ was taken as zero. The biggest factor on this uncertainty is temperature and this is the parameter being measured. The changes in the resistance of the sensor are related to the temperature being measured.

The overall uncertainty $U_{overall}$ was therefore determined from equation (15) as ± 0.446 ºC.

4.2 Predicted (Theoretical) Air flow

The temperatures at various sections of the dryer are presented first, as thermal buoyancy which creates the air flow in the dryer depends on these temperatures. Figures 3, 4 and 5 show the variation of temperature with elapsed drying time from the drying experiments for the mixed-mode 10 kg, indirect-mode 10 kg and mixed-mode 5 kg drying, respectively. The air temperature in the grain bed increases from a value almost equal to ambient temperature and rises to one close to the temperature of air exiting the collector and entering the grain bed. This is due to the grain gaining sensible heat from hot air exiting the collector and entering the grain bed. Figure 4 shows the air temperature on top of the grain bed in the indirect-mode 10 kg dropping to values below ambient temperature in the first hour of drying which is not seen in Figure 3 and 5. Condensation of moisture laden air from the grain bed as it came into contact with the cooler space above the grain bed might have lowered the temperature. This situation did not happen in the mixed-mode 10 kg and 5 kg (Figure 3 and 5) due to the heating of the top of the grain bed by direct radiation, which in turn heated the air coming out of the grain bed to temperatures above ambient.

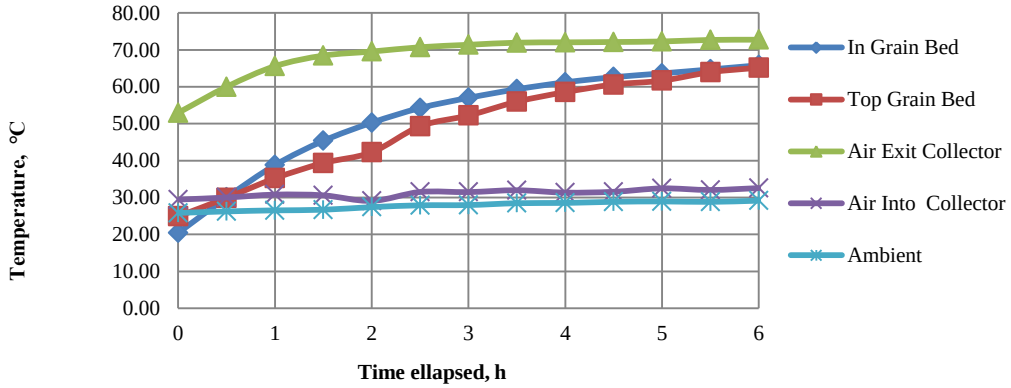

Figure 3. Temperatures at various sections of the dryer for the Mixed-mode 10 kg capacity

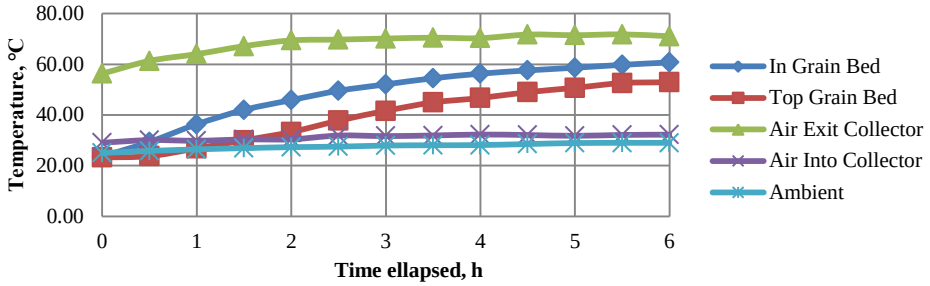

Figure 4. Temperatures at various sections of the dryer for the Indirect-mode 10 kg

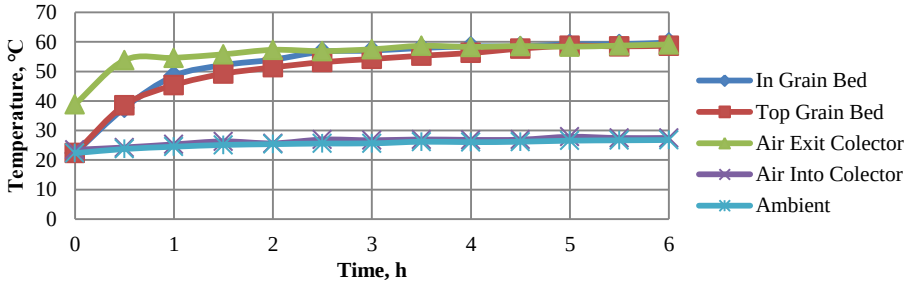

Figure 5. Temperatures at various sections of the dryer for the Mixed-mode 5 kg

Figures 6, 7 and 8 show the variation of the predicted thermal buoyancy at the various sections of the dryer. The thermal buoyancy within the collector, below the grain bed and in the grain bed are fairly constant from one hour to the end of drying. However, the thermal buoyancy created on top of the grain bed for the mixed-mode drying (Figure 6 and 8) is higher than that below the grain bed (at collector exit). This is due to the additional heating of the air on top of the grain bed by direct radiation on top of the grain bed. The thermal buoyancy in the mixed-mode 10 kg (Figure 6) is slightly higher than that in the indirect-mode 10 kg (Figure 7) and this contributes to higher air flow for the mixed-mode compared to the indirect-mode.

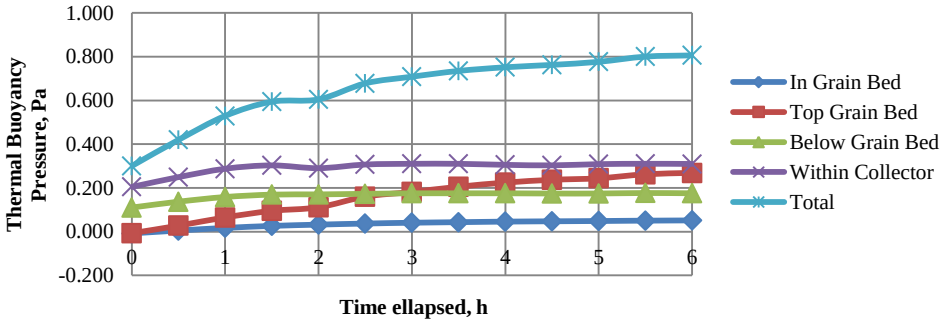

Figure 6. Thermal Buoyancy at various sections of the dryer for the Mixed-mode 10 kg

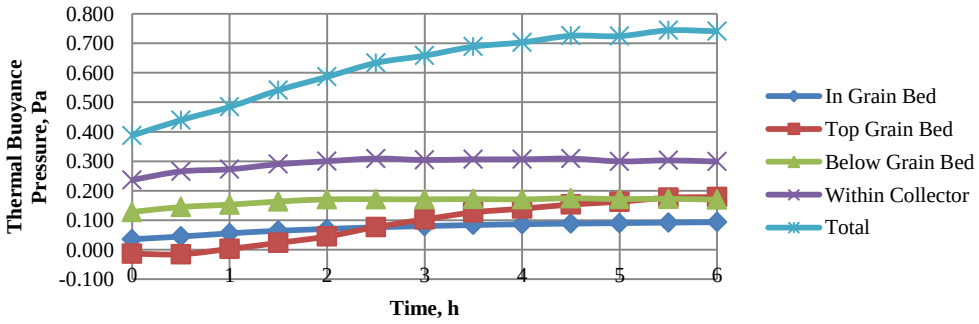

Figure 7. Thermal Buoyancy at various sections of the dryer for the Indirect-mode 10 kg

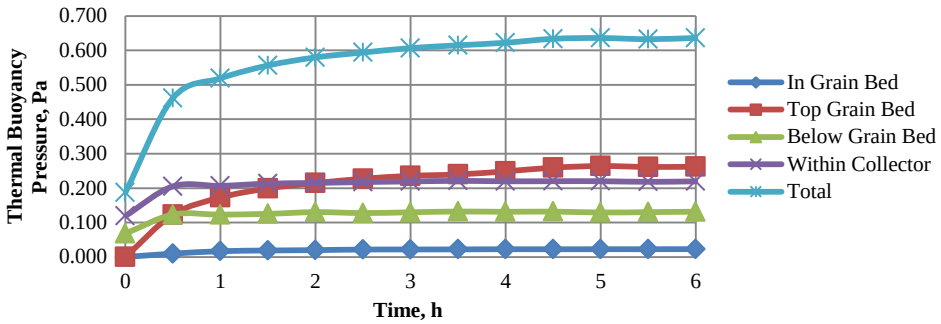

Figure 8. Thermal Buoyancy at various sections of the dryer for the Mixed-mode 5 kg

Figures 9, 10 and 11 show the pressure drops at various sections of the dryer for the mixed-mode 10 kg, indirect-mode 10 kg and mixed-mode 5 kg, respectively. The pressure drop through the grain bed is dominant, whereas that within the collector, at collector exit and dryer exit are very small and can be neglected. This is in agreement with most other works on natural convection solar drying (Exell, 1980; Jindal & Gunasekaran, 1982; Oosthuizen, 1987) who reported that the pressure drop across the grain bed is the dominant one in the dryer, that the resistance to air flow due to other dryer components is negligible due to the small air flow involved.

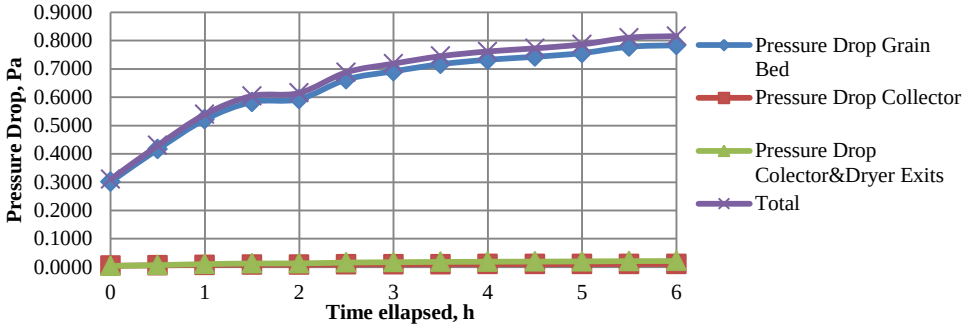

Figure 9. Pressure Drop at various sections of the dryer for the Mixed-mode 10 kg

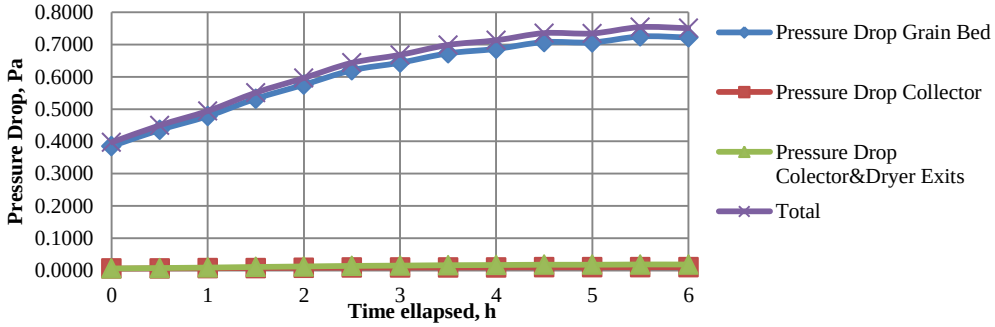

Figure 10. Pressure Drop at various sections of the dryer for the Indirect-mode 10 kg

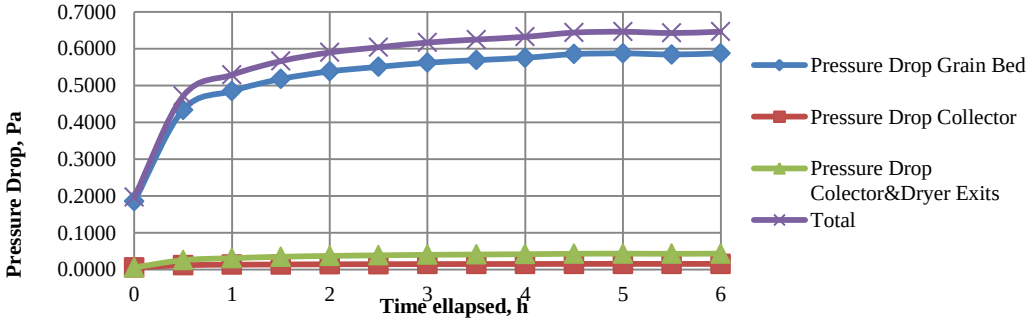

Figure 11. Pressure Drop at various sections of the dryer for the Mixed-mode 5 kg

Figure 12 shows the theoretical (model) mass air flow rates for the mixed-mode 10kg, indirect-mode 10 kg and mixed-mode 5 kg. The air flow rates increase rapidly in the first hour of drying then become constant during the last hour of drying. As the grain dries, there is less heat used in evaporating moisture from the grain, resulting in more heat contributing to the thermal buoyancy through the temperature of air on top of the grain bed, resulting in an increase in air flow from beginning to the end of drying. The mixed-mode 5 kg bed has the highest air flow as it offers the least resistance to air flow due to the thinner bed depth. For the 10 kg grain beds, the mixed-mode has a higher air flow than the indirect-mode due to the additional heating of the top of the grain bed in the mixed-mode. Although the difference in air flow between the mixed-mode and indirect-mode is very small, with a mean difference of 0.0003kg/s as given in Table 1., when the dryer is operated over a six-hour period of drying, the difference in moisture content at the end of drying may be substantial, with the air flow having contributed to the difference.

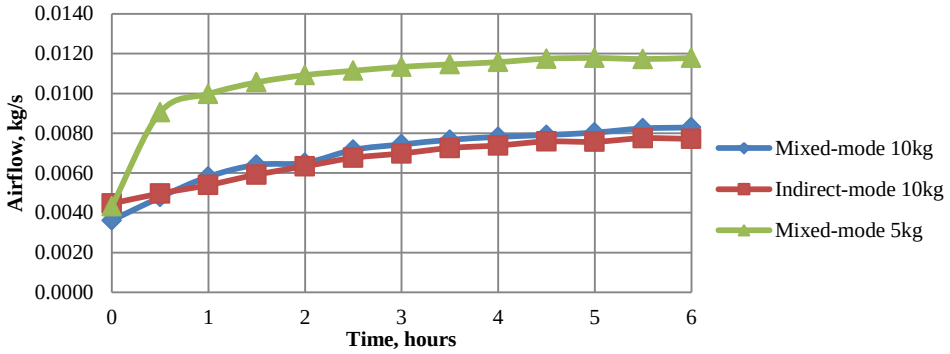

Figure 12. Theoretical (Model) mass Air flow rates for the Mixed-mode 10kg, Indirect-mode 10kg and Mixed-mode 5kg

Table 1. Mean theoretical air flow in the dryer with capacity 10kg

Mixed-mode air flow (kg/s)	Indirect-mode air flow (kg/s)	Mean Difference in air flow (kg/s)
0.0069	0.0066	0.0003

4.3 Measured Air Flow

The graphs of temperature difference during the heater on and off times are shown in Figures 13 and 14 for the mixed-mode 10 kg and mixed-mode 5 kg, respectively. From the graphs, the rise in temperature difference when the heater is on can be clearly seen. One would have expected that the temperature difference during the time the heater is off would be zero because the air inside the box is not heated. This however, is not the case. The above zero temperature difference experienced when the heater is off may be caused by the top end of the heater box conducting some heat from the collector since the two are physically joined together. There could also be some heat gain from the lights of the solar simulator to the heater box.

The temperature difference does not reach the maximum operating point immediately the heater is switched on. It also does not drop back to the off value immediately after switching off the heater. The reason for the first observation could be that the heated air has to travel a short distance from the heater wire to the hot junctions before its effect can be registered. In the second case, the heater wire takes a bit of time to drop its temperature from the operating one to that of the air surrounding it.

In general the temperature difference at 50 mm is higher than at other positions. This is reasonable as hot air is less dense than cold air and therefore rises above the cooler air. This however, does not imply that the air inside the collector has the same temperature distribution across the air gap. The absorber is the hottest part of the collector and one would expect the air nearer to it to be hotter than at other positions.

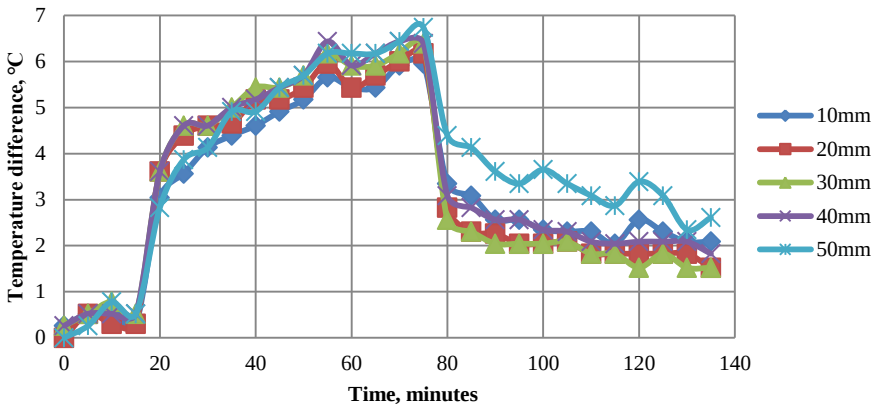

Figure 13. Temperature difference between the hot and cold thermocouple junctions for the Mixed-mode 10 kg at different positions from the bottom of the heater box

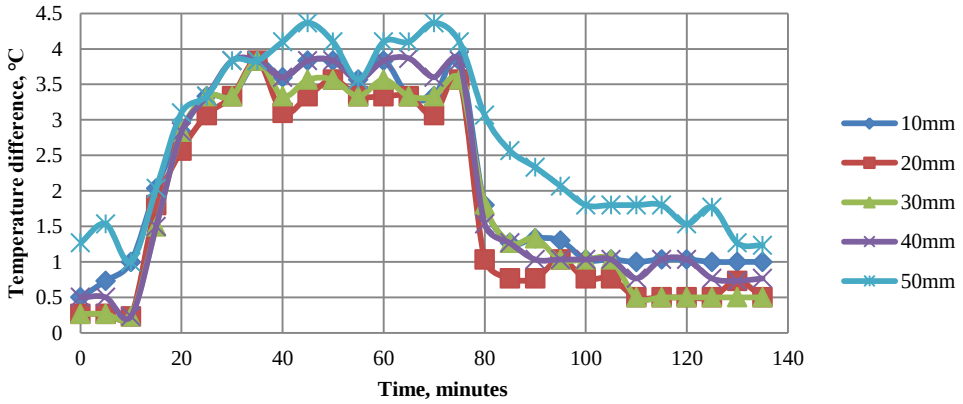

Figure 14. Temperature difference between the hot and cold thermocouple junctions for the Mixed-mode 5 kg at different positions from the bottom of the heater box

The experimental values of mass air flow rate calculated from the measured temperature differences from the graphs are given in Table 2 for the mixed-mode 10 kg and 5 kg capacities. The air flow for 5 kg bed is higher than that for the 10 kg. This is reasonable because the 5 kg offers less resistance to air flow than the 10 kg.

Table 2. Experimental and theoretical (model) air flow for mixed-mode 10 kg and 5 kg capacities

Capacity [kg]	Experimental Air flow [kg/s]	Theoretical Air flow [kg/s]
5	0.0132	0.0043 – 0.0119
10	0.0088	0.0036 – 0.0083

Table 2 also shows the air flows predicted by the model. For the model, the air flows have a range with the smallest values at the beginning of the drying experiment and the maximum values at the end of the drying experiment. The model air flow values at the end of the drying experiments (0.0119 kg/s for the 5 kg and 0.0083 kg/s for the 10 kg) are in very good agreement with measured air flows (0.0132 kg/s for the 5 kg and 0.0088 kg/s for the 10 kg). Towards the end of the drying, in the last one hour, the grain is almost dry and its moisture content is almost equal to that used in the air flow experiment. These mass flow values are reasonable for this size (1.2 m * 1.0 m) of collector. Othieno (1987) used a collector of 2 m * 1 m and measured the air velocity with an air velocity meter at a chimney cross-section of 0.2 m * 0.2 m. He obtained air speed of 0.05 to 0.3 m/s which can be converted to give mass flow values of 0.0021 to 0.0123 kg/s. Bala and Woods (1994) simulated a collector of 2 m * 1.5 m and predicted mass flow values of 0.006 to 0.1 kg/s. Berinyun et al. (2012) estimated the air flow through a natural convection solar tunnel dryer to be 9.68 m^3/h which can be converted to give mass air flow of 0.0029 kg/s. Therefore the air flow rates obtained in this work are within the range of those obtained by other researchers as cited above.

5. Conclusions

An air flow model for natural convection mixed-mode and indirect-mode solar drying of maize grain has been developed by balancing the sum of the individual thermal buoyancy pressures with the pressure drops at the various sections of the dryer. The air flow predicted by the model has been found to be in good agreement with measured air flow from drying experiments.

Analysis of the results show that the thermal buoyancy on top of the grain bed is largely responsible for the variation in air flow, translating into low mass air flow during the early stages of drying when grain moisture content is high, and higher air flow in the later stages when grain moisture content is low. It would be useful in future to look at how the air flow in the early stages of drying can be increased. One way is to increase the thermal buoyancy in the collector as it is the biggest contributor to the mass air flow and is fairly constant throughout the drying period. The model also shows that the heating of the top of the grain bed in the mixed-mode translates into a higher air flow rate than the indirect-mode although the difference is small.

A comparison of the pressure drops at the various sections of the dryer show that the pressure drop across the grain bed is dominant and offers the highest resistance to the air flow rate, implying that the other pressure drops can be neglected in the model.

The model can be used to predict air flow in natural convection solar drying of other grains after replacing the grain specific equation for pressure drop in the grain bed, with that of the grain under consideration.

Acknowledgments

The author wishes to acknowledge the funding from the University of Zambia which made it possible for the research to be carried out.

References

Al-Neama, M. A., & Farkas, I. (2016). Influencing of Solar Drying Performance by Chimney Effect. *Hungarian Agricultural Engineering***,** no. 30/2016, 11-16. https://doi.org/10.17676/HAE.2016.30.11

Bala, B. K., & Woods, J. L. (1994). Simulation of the Indirect Natural Convection Solar Drying of Rough Rice. *Solar Energy, 53*(3), 259-266. https://doi.org/10.1016/0038-092X(94)90632-7

Bayazitoglu, Y., & Ozisik, M. N. (1988). *Elements of Heat Transfer*. New York: McGraw Hill.

Benson, J. M. (1974). Survey of Thermal Devices for Measuring Flow. In R. B. Dowdell (Ed.), *Flow: Its Measurement and Control in Science and Industry*, *1*(2). Flow Measuring Devices, Instrument Society of America.

Berinyuy, J. E., Tangka, J. K., & Weka Fotso, G. M. (2012). Enhancing Natural Convection Solar Drying of High Moisture Vegetables with Heat Storage. *Agric Eng Int: CIGR Journal*, *14*(1), 141-148. Retrieved from http://www.cigrjournal.org

Brenndorfer, B., Kennedy, L., Oswin, B., Trim, D. S., Mrema, G. C., & Werekop, C. (1987). *Solar Dryers, their Role in Post-harvest Processing.* Common Wealth Secretariat, Malborough House, Pall Mall, London, U.K.

Brooker, D. B. (1969). Computing Air Pressure and Velocity Distribution when Air flows through a Porous Medium and Nonlinear Velocity-Pressure Relationship exist. *Transactions of the ASAE, 12*, 118-120. https://doi.org/10.13031/2013.38776

Brooker, D. B., Bakker-Arkema, F. W., & Hall, C. W. (1992). *Drying and Storage of Grains and Oilseeds*. AVI Van Nostrand Reinhold, New York, 1992.

Daly, B. B. (1979). *Woods Practical Guide to Fan Engineering*. Woods of Colchester Limited, United Kingdom. ASIN: B001E3OVZW.

Dunn, W. C. (2006). *Introduction to Instrumentation, Sensors, and Process Control*. Retrieved from http://myprojectforu.weebly.com/uploads/6/3/6/7/6367594/introduction_instrumentationsensors_controlsystems.pdf

Exell, R. H. B. (1980). Basic design theory for a simple solar rice dryer. *Renewable Energy Review Journal, 1*, 1-14. Retrieved from http://www.rericjournal.ait.ac.th/index.php/reric/article/view/1654

Jindal, V. K., & Gunasekaran, S. (1982). Estimating Airflow and Drying Rate due to Natural Convection in Solar Rice Dryers. *Renewable Energy Review Journal*, *4*(2), 1-9. Retrieved from http://www.rericjournal.ait.ac.th/index.php/reric/article/view/1634

Maundu, N. M., Kiptoo, K. S., Eliud, K., Kindole, D., & Nakajo, Y. (2017). Air-flow Distribution Study and

Performance Analysis of a Natural Convection Solar Dryer. *American Journal of Energy Research*, *5*(1), 12-22. Retrieved from http://article.scienergyresearch.com/pdf/AJER-5-1-2.pdf

Moffat, R. J. (1988). Describing the Uncertainties in Experimental Results. *Experimental Thermal and Fluid Science*, *1*, 3-17. https://doi.org/10.1016/0894-1777(88)90043-X

National Aeronautics and Space Administration. (2010). Measurement Uncertainty Analysis Principles and Methods - *NASA Measurement Quality Assurance Handbook* – ANNEX 3, NASA-HDBK-8739.19-3, National Aeronautics and Space Administration, Washington DC 20546. Retrieved from https://standards.nasa.gov/standard/nasa/nasa-hdbk-873919-3

Oosthuizen, P. H. (1987). A Numerical Model of a Natural-Convection Solar Grain Dryer: Development and Validation. Proceedings of *a Workshop held in Dakar, Senegal*, IDRC, Canada, 234-251. Retrieved from https://idl-bnc-idrc.dspacedirect.org/bitstream/handle/10625/8557/IDL-8557.pdf?sequence=1

Othieno, H. (1987). Circulation of Air in Natural-Convection Solar Dryers. *Proceedings of a Workshop held in Dakar, Senegal, IDRC, Canada*, 47-59. Retrieved from https://idl-bnc-idrc.dspacedirect.org/bitstream/handle/10625/17684/IDL-17684.pdf?sequence=1

Rigit, A. R. H., & Low, P. T. K. (2010). Heat and Mass Transfer in a Solar Dryer with Biomass Backup Burner. *International Journal of Mechanical, Engineering*, *4*(2). World Academy of Science, Engineering and Technology, Aerospace, Industrial, Mechatronic and Manufacturing. https://doi.org/10.5281/zenodo.1329412

Simate, I. N. (1999). *Mixed Mode Solar Drying* (Unpublished Ph.D. Thesis). University of Newcastle upon Tyne, United Kingdom.

Simate, I. N. (2001). Simulation of the Mixed-Mode Natural-Convection Solar Drying of Maize. *Drying Technology - An International Journal*, *19*(6), 1137-1155. https://doi.org/10.1081/DRT-100104810

Vintilă, M., Ghiauș, A. G., & Fătu, V. (2014). Prediction of Air Flow and Temperature Profiles inside Convective Solar Dryer. *Bulletin UASVM Food Science and Technology, 71*(2). https://doi.org/10.15835/buasvmcn-fst:10868